Dalton Transactions

PAPER

View Article Online
View Journal | View Issue

Cite this: *Dalton Trans.*, 2014, **43**, 5190

Assembly and core transformation properties of two tetrahedral clusters: $[Fe^{III}_{13}P_8W_{60}O_{227}(OH)_{15}(H_2O)_2]^{30-}$ and $[Fe^{III}_{13}P_8W_{60}O_{224}(OH)_{12}(PO_4)_4]^{33-}$†

Pedro I. Molina, Haralampos N. Miras, De-Liang Long and Leroy Cronin*

Received 1st December 2013,
Accepted 29th January 2014

DOI: 10.1039/c3dt53382d

www.rsc.org/dalton

Two nanosized 2.6 nm Fe^{III} substituted polyoxotungstates $[Fe^{III}_{13}P_8W_{60}O_{227}(OH)_{15}(H_2O)_2]^{30-}$ (**1**) and $[Fe^{III}_{13}P_8W_{60}O_{224}(OH)_{12}(PO_4)_4]^{33-}$ (**2**) are presented herein. Both clusters are synthesized from the reactions of trilacunary polyoxotungstate precursor $[\alpha\text{-}P_2W_{15}O_{56}]^{12-}$ and $FeCl_3$ under strict pH control at atmospheric pressure. The compounds are fully characterised in the solid state (FTIR and single-crystal XRD, elemental and thermogravimetric analyses), solution (cyclic voltammetry and UV-Vis spectroscopy) and in the gas phase (ESI-MS). An $\{Fe^{III}_{13}\}$ core is present in both clusters which can be described as Archimedean solids (truncated tetrahedron, **1**; elongated cuboctahedron, **2**). **1** shows iron delivery properties coupled to a K^+-triggered transformation of the $\{Fe_{13}\}$ core to a $\{K\subset Fe_{12}\}$ core in solution. Cyclic voltammetry shows the presence of independent W- and Fe-centred redox processes that support the stability of the clusters in solution. ESI-MS analyses confirm further the stability of **1** and **2** in the gas phase.

Introduction

Transition metal substituted polyoxometalates (TMSPs) constitute an important subset of the polyoxometalate (POM) family owing to their wide structural diversity and remarkable physical properties.[1] One of the most favoured synthetic approaches employed to access new structures consist of reacting preformed lacunary species with transition metal salts in solution under strict control of key synthetic parameters, *i.e.* pH, ionic strength and concentration of structure directing agents.[2] This strategy has proven to be highly successful for the assembly of new polyanions of great structural diversity and wide range of nuclearities.[3] In particular, the use of the trilacunary $[\alpha\text{-}P_2W_{15}O_{56}]^{12-}$ ($\{P_2W_{15}\}$) heptadentate ligand in controlled reaction systems involving several first-row transition metals has led to the isolation of a number of TMSPs. The structures of these assemblies range from the classic sandwich, Weakley-type, topology to trimeric clusters, $[(PO_3)_2\{\alpha\text{-}Co^{II}_3P_2W_{15}O_{51}(OH)(H_2O)_2\}_3]^{27-}$,[4] and tetrameric assemblies such as $[Co^{II}_{14}P_{10}W_{60}O_{232}(OH)_9(H_2O)_6]^{35-}$,[4] a polyanion which displays a highly unusual cross-shaped topology. Interestingly, four $\{P_2W_{15}\}$-based TMSPs display an overall tetrahedral geometry which replicates the symmetry of the templating $[PO_4]^{3-}$ heteroanion in the $\{P_2W_{15}\}$ unit and therefore are labelled as "supertetrahedral" cluster assemblies. Three of these four clusters are Ti^{IV}-substituted polyanions, $([(\alpha\text{-}Ti^{IV}_3P_2W_{15}O_{60.5})_4Cl]^{37-}$,[5] $[(\alpha\text{-}Ti^{IV}_3P_2W_{15}O_{62})_4\{\mu_3\text{-}Ti(OH)_3\}Cl]^{45-}$,[6] and $([(\alpha\text{-}Ti^{IV}_3P_2W_{15}O_{57.5}(OH)_3)_4]^{24-}$[7] while the fourth one is an Fe^{III}-substituted cluster, $[KFe_{12}(OH)_{18}(\alpha\text{-}1,2,3\text{-}P_2W_{15}O_{56})_4]^{29-}$, which was reported by us some years ago.[8] Furthermore, this latter cluster represents the only reported example of an $Fe^{III}/\{P_2W_{15}\}$ polyanion exhibiting nuclearity higher than four.

Nevertheless, the number of reported oligomeric TMSPs based on other lacunary precursors (*i.e.* $\{XW_9\}$) is still much greater than the number of $\{P_2W_{15}\}$-based TMSPs. Consequently, it became apparent to us that there should be more undiscovered TMSP architectures based on this lacunary precursor which evaded detection due to incomplete mapping of the reaction conditions. Intrigued by this observation, we decided to investigate the parameter space of $Fe^{III}/\{P_2W_{15}\}$ reaction systems in a quest to identify the reaction coordinates which direct the self-assembly process of high-nuclearity clusters with potential novel functionalities.

In particular, we decided to scan the pH value of $Fe^{III}/\{P_2W_{15}\}$ reaction mixtures based on the effect of this synthetic parameter in the formation of the aforementioned $Co^{II}/\{P_2W_{15}\}$ high-nuclearity clusters. Moreover, a careful

School of Chemistry, University of Glasgow, Glasgow, UK.
E-mail: L.Cronin@chem.gla.ac.uk; Fax: +44 (0) 141 330 4888;
Tel: +44 (0) 141 330 6650

† Electronic supplementary information (ESI) available: Experimental and instrumentation details, crystal structures, CV, FTIR, TGA, UV-Vis, ESI-MS, BVS. See DOI: 10.1039/c3dt53382d

analysis of the reported synthesis of $[KFe^{III}_{12}(OH)_{18}(\alpha\text{-}1,2,3\text{-}P_2W_{15}O_{56})_4]^{29-}$, hitherto the only example of a large $Fe^{III}/\{P_2W_{15}\}$ cluster, provides a significant insight in support of that approach. An initial step in the formation of the cluster must be the release of acrylate ligands by the $\{Fe^{III}_3\}$ complex used as the starting material, $[Fe^{III}_3(\mu_3\text{-}O)(CH_2{=}CHCOO)_6(H_2O)_3]Cl{\cdot}7H_2O$, in the presence of the more strongly nucleophilic $\{P_2W_{15}\}$ clusters. This free acrylate subsequently hydrolyses (pK_a = 4.50) in the aqueous reaction mixture, a process that produces the hydroxo ligands which finally bridge the $\{Fe^{III}_3P_2W_{15}\}$ units in the supertetrahedral structure. This tendency of monomeric Fe^{III}-substituted clusters to assemble into larger structures *via* $\{Fe^{III}\text{–}OH\text{–}Fe^{III}\}$ bridges has been previously observed in reaction systems involving lacunary Keggin ligands.[9]

The implementation of this synthetic programme led to the discovery of two nanosized polyoxometalate assemblies incorporating $\{Fe^{III}_{13}\}$ cores and stabilized by $\{P_2W_{15}\}$ ligands which are presented herein. $Na_{30}[Fe^{III}_{13}P_8W_{60}O_{227}(OH)_{15}(H_2O)_2]$ (Na_{30}-**1**) has a central $\{Fe^{III}_{12}\}$ core closely related to the one in $[KFe^{III}_{12}(OH)_{18}(\alpha\text{-}1,2,3\text{-}P_2W_{15}O_{56})_4]^{29-}$ (**3**) and the aforementioned $Ti^{IV}/\{P_2W_{15}\}$ clusters while $Na_{33}[Fe^{III}_{13}P_8W_{60}O_{224}(OH)_{12}(PO_4)_4]$ (Na_{33}-**2**) incorporates a Fe^{III} core structurally analogous to the cores found in other Fe^{III} complexes supported by $\{PW_9\}$[10] and $\{AsW_9\}$ ligands.[11] The $\{Fe^{III}_{13}\}$ cores present in both clusters can both be envisaged as two separate units, *i.e.* a $\{Fe^{III}_{12}\}$ motif in which the Fe^{III} centres occupy the vacant positions in the $\{P_2W_{15}\}$ starting material and an additional, "exolacunary", Fe^{III} centre, trapped by $\{Fe^{III}_{12}\}$ unit but located outside the vacant positions of the $\{P_2W_{15}\}$ ligands.

1 transforms in solution into **3** as a result of the selective encapsulation of a potassium cation and the concomitant expulsion of an Fe^{III} centre to the aqueous solution. It is also worth noting that, to the best of our knowledge, this is the first example of a large TMSP undergoing a change of nuclearity of its 3d metal-oxo core in solution triggered by a selective cation- exchange reaction whilst retaining their overall structural integrity. Fig. 1 shows a representation of the molecular structures of **1** and **2**.

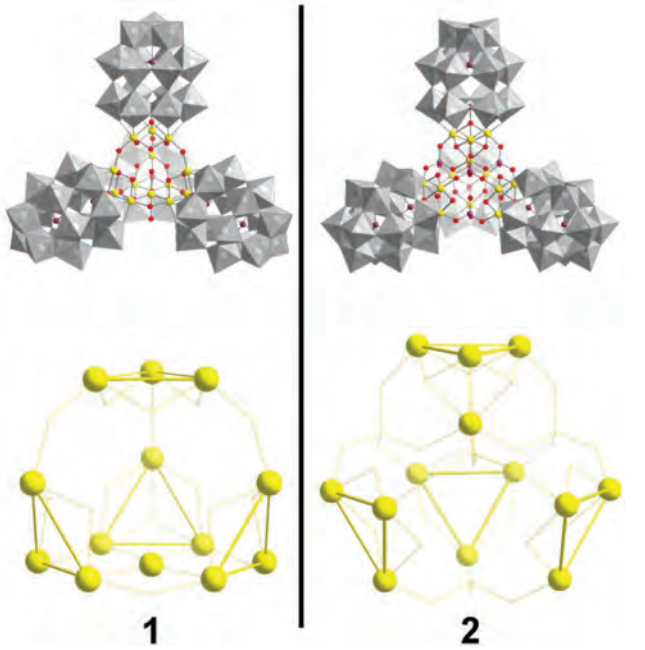

Fig. 1 Top: Molecular structures of $[Fe^{III}_{13}P_8W_{60}O_{227}(OH)_{15}(H_2O)_2]^{30-}$ (**1**, left) and $[Fe^{III}_{13}P_8W_{60}O_{224}(OH)_{12}(PO_4)_4]^{33-}$ (**2**, right). Bottom: combined ball-and-stick/wireframe representation of the $[\{Fe^{III}(H_2O)_2\}\subset\{Fe^{III}_{12}O_3(OH)_{15}\}]^{18+}$ core in **1** (left) and of the $[Fe^{III}\subset\{(PO_4)_4Fe^{III}_{12}O_3(OH)_9\}]^{12+}$ in **2** (right). Colour code: WO_6, grey polyhedra; O, red; Fe^{III}, yellow; P, plum.

Results and discussion

Synthesis

$Na_{30}[Fe^{III}_{13}P_8W_{60}O_{227}(OH)_{15}(H_2O)_2]{\cdot}56H_2O$ (Na_{30}-**1**) was isolated from a deep red NaCl aqueous solution (pH = 5.0) containing a mixture of $\{P_2W_{15}\}$ and Fe^{III} in a 1 : 2.6 molar ratio. Under similar reaction conditions, but in the presence of a small amount of phosphoric acid, $Na_{33}[Fe^{III}_{13}P_8W_{60}O_{224}(OH)_{12}(PO_4)_4]{\cdot}67H_2O$ (Na_{33}-**2**) was isolated from a light brown solution. Both compounds crystallised overnight as dark red hexagonal plates (Na_{30}-**1**) and light brown blocks (Na_{33}-**2**) suitable for full crystallographic characterization. This multistep synthetic strategy, whereby a lacunary cluster precursor is reacted with simple metal salts in aqueous solution, has proven to be a successful approach to prepare structurally diverse and oligomeric TMSPs.[3] In the case of the title compounds, a likely sequence of events during their assembly includes the initial formation of the $\{Fe^{III}_3P_2W_{15}\}$ monomer, occurring upon the addition of $\{P_2W_{15}\}$ to the aqueous ferric solution, followed by the condensation of four of these monomers into the final structures, a process induced by the addition of the inorganic base to the reaction mixture. The role of the base is slightly different in both synthetic procedures, *i.e.* acting directly as the supplier of the ligands connecting the four $\{Fe^{III}_3P_2W_{15}\}$ units (**1**) or indirectly by deprotonating the phosphoric acid to form the bridging ligands in **2**.

The structure of **1**, in particular the position of the exolacunary Fe^{III} centre which is located at one of the four "windows" of the supertetrahedral assembly, encouraged us to explore several modified synthetic procedures aiming to increase the nuclearity of the $\{Fe^{III}_{13}\}$ core. In this way, a series of reactions were performed in which the Fe^{III} : $\{P_2W_{15}\}$ molar ratio was increased to values ranging between 2.7 and 5.0. Unfortunately, no crystalline material was obtained from these mixtures. Similarly, in order to induce further fragmentation of the $\{Fe^{III}_3P_2W_{15}\}$ units and hence generate other building blocks in the reaction mixtures, a number of reactions were conducted using the same starting materials albeit adjusting the pH to values higher than 6.0. However, these reactions resulted solely in the formation of amorphous solid precipitates.

Regarding the synthesis of **2**, the molar ratio of H_3PO_4/Fe^{III} and the sequence of the addition of reagents seem to play an

Table 1 Summary of the different yields (%) obtained in relation to two key synthetic parameters, *i.e.* the sequence of reagent addition and the H_3PO_4 : Fe^{III} molar ratio (*R*), for the synthesis of **2**

Addition sequence	*R*	Yield (%)
$FeCl_3/\{\alpha\text{-}P_2W_{15}\} \rightarrow H_3PO_4$	27.0	14
$H_3PO_4/FeCl_3 \rightarrow \{\alpha\text{-}P_2W_{15}\}$	27.0	28
$H_3PO_4/FeCl_3 \rightarrow \{\alpha\text{-}P_2W_{15}\}$	81.1	3
	54.1	7
	27.0	28

important role in the successful formation of the cluster, namely, the yield of **2** doubles if the aqueous H_3PO_4 solution is added to the reaction mixture prior to the addition of the $\{P_2W_{15}\}$ ligand. Furthermore, in reactions where the aqueous H_3PO_4 is added first to the NaCl solution, a trend can be observed whereby an increase in yield seems to correlate to a decrease of the H_3PO_4/Fe^{III} molar ratio (*R*) adjusted for a particular reaction mixture. Table 1 summarises the relationship between these values and the addition sequence of reagents.

Compound **1** can be transformed into **3** in acidified aqueous solution in the presence of potassium ions. When red crystals of Na_{30}-**1** were added to a volume of 0.1 M aqueous KCl solution (pH = 3.0), a thick yellow suspension was produced which, upon heating, turned into a bright yellow clear solution. Yellow–green crystals of **3** formed overnight as confirmed crystallographically by several checks of the unit cell dimensions. The driving force for this transformation seems to be the stronger interactions in **3** between the central K^+ ion and the surrounding hydroxo ligands than between those same ligands and the central water molecule in **1**. The interatomic distances between those hydroxo ligands and the central atom in both cases range from 3.0 Å to 3.1 Å, values which are too high for hydrogen bonding with the aqua ligands yet in the range for coordinative bonding between the potassium centre and those hydroxo ligands. The disassembly and reassembly of the cluster does not seem to be required for the transformation as the approximate diameter of the "windows" formed by the three hydroxo ligands coordinating the exolacunary Fe in equatorial positions is greater than the atomic diameter of the K^+ ion. Hence, the structure of the cluster is presumably maintained during the exchange of the trapped Fe^{III} by the K^+ in solution. Scheme 1 summarises the key synthetic parameters regulating the formation of the title compounds and the transformation of **1** to **3**.

Structure

1 and **2** (Table 2) can be structurally envisaged as tetrameric assemblies of four plenary $\{Fe^{III}{}_3P_2W_{15}\}$ units displaying a tetrahedral geometry in which an exolacunary Fe^{III} centre is trapped by a $\{Fe^{III}{}_{12}\}$ core. The $\{Fe_{13}\}$ core in **2** has been found in two polyanions albeit supported by different lacunary ligands, namely, $\{A\text{-}\alpha\text{-}PW_9\}/[PO_4]^{3-}$ in the compounds reported separately by Dolbecq's[10a] and Yang's[10b] groups, and $\{A\text{-}\alpha\text{-}AsW_9\}/[AsO_4]^{3-}$ in the cluster reported by Wang *et al.*[11] Moreover, the oxidation state of the exolacunary iron centre is 2+ in all three clusters as opposed to 3+ in **1** and **2**. Other relevant tetrameric TMSPs assemblies supported by different trilacunary ligands showing an overall tetrahedral geometry are the single-molecule

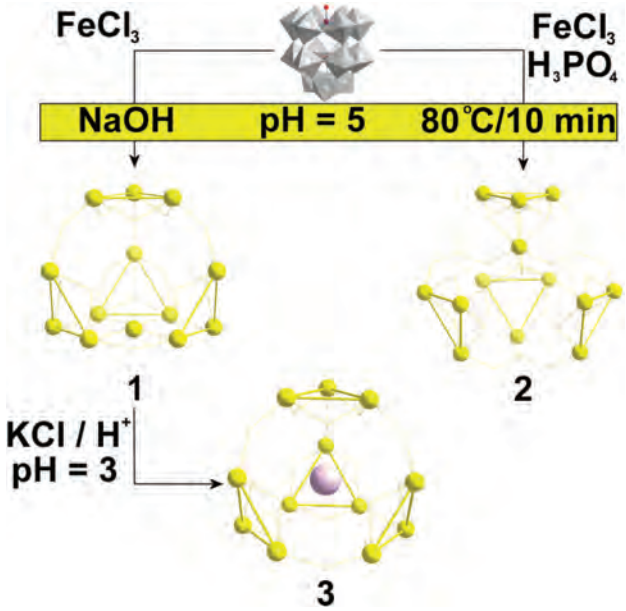

Scheme 1 Summary of key synthetic parameters required for the formation of **1** and **2** from $[\alpha\text{-}P_2W_{15}O_{56}]^{12-}$ and for the transformation of **1** into **3**.

Table 2 Crystallographic data for $Na_{30}[\mathbf{1}]\cdot 56H_2O$ and $Na_{33}[\mathbf{2}]\cdot 67H_2O$[a]

	$Na_{30}[\mathbf{1}]\cdot 56H_2O$	$Na_{33}[\mathbf{2}]\cdot 67H_2O$
Formula	$Fe_{13}H_{131}Na_{30}O_{300}P_8W_{60}$	$Fe_{13}H_{146}Na_{33}O_{319}P_{12}W_{60}$
M_r (g mol^{-1})	17 626.55	18 138.53
Space group	$R\bar{3}$	$P\bar{1}$
Crystal system	Trigonal	Triclinic
a (Å)	29.7437(10)	24.8202(3)
b (Å)	29.7437(10)	27.1921(4)
c (Å)	76.260(4)	31.4135(4)
α (°)	90	70.5521(12)
β (°)	90	86.2853(9)
γ (°)	120	69.6989(12)
V (Å^3)	58 427(5)	18 719.0(4)
Z	6	2
μ (mm^{-1})	18.258	19.024
Refl. coll.	257 860	292 534
Indep. refl.	25 553	73 428
R(int)	0.0563	0.0927
GooF on F^2	1.224	1.027
$R_1[I > 2\sigma(I)]$	0.0503	0.0583
$wR_2[I > 2\sigma(I)]$	0.1277	0.1303
R_1 (all data)	0.0784	0.1127
wR_2 (all data)	0.1602	0.1608

[a] X-ray diffraction data for single crystal structure determination was collected on an Oxford Diffraction Gemini Ultra [λ(Mo K_α) = 0.71073 Å] equipped with an ATLAS CCD detector. Corrections for incident and diffracted beam absorption effects were applied *via* analytical numeric absorption correction with a multifaceted crystal model[24] or empirical absorption correction.[25] Structure solution and refinement were performed by using SHELXS-97[26] and SHELXL-97[26] integrated in the WINGX[27] system. Crystallographic details for **1** and **2** may be obtained from CSD quoting CCDC 425939 and 425940 respectively.

magnet $[\{Co^{II}_4(OH)_3PO_4\}_4(B\text{-}\alpha\text{-}PW_9O_{34})_4]^{28-}$ [12] and the mixed-valence $[Mn^{III}_{13}Mn^{II}O_{12}(PO_4)_4(B\text{-}\alpha\text{-}PW_9O_{34})_4]^{31-}$.[13] Clusters showing an idealised square planar[10a,4] or a distorted tetrahedral topology have also been isolated.[14]

The molecular structure of **1** can be described as an assembly of four $\{Fe^{III}_3P_2W_{15}\}$ units, connected by six $\{\mu_2\text{-OH}\}$ bridging ligands, which traps an exolacunary Fe^{III} centre. The position of this Fe^{III} centre is statistically disordered over four crystallographic positions located at the centre of the triangles defined by three neighbouring oxo ligands belonging to separate $\{\alpha\text{-}Fe^{III}_3P_2W_{15}\}$ units. The overall symmetry of the cluster is an idealised C_{3v} where the C_3 axis is located on the imaginary line joining the two P^V centres in one of the $\{P_2W_{15}\}$ units and the opposite exolacunary Fe^{III} centre. Therefore, the presence of this Fe^{III} centre lowers the overall symmetry of the cluster from the idealised T_d observed in **3** to a C_{2v}. Two representations of the molecular structure of **1** are shown in Fig. 2.

An alternative way of describing **1** involves isolating the central Fe-oxo core from the $\{\alpha\text{-}P_2W_{15}\}$ units. Hence, this $\{Fe_{13}O_{20}\}$ core is formulated as $[\{Fe^{III}(H_2O)_2\}\subset\{Fe^{III}_{12}O_3(OH)_{15}\}]^{18+}$ on the basis of BVS (see ESI†), electrochemical and microanalytical considerations together with the absence of a reducing agent in both reaction mixtures. A representation of this $\{Fe^{III}_{13}\}$ is given in Fig. 3. The presence of an Fe^{II} centre in the aforementioned $\{Fe_{13}\}/\{PW_9\}$[10] and $\{Fe_{13}\}/\{AsW_9\}$[11] clusters is explained by the role of the different organic amines in the reaction mixtures which, under the hydrothermal conditions imposed during the synthesis, are able to reduce the Fe^{III} centres. In the case of the title compounds, no amines or any other organic species are part of the reaction mixtures and, moreover, the solutions are vigorously stirred under aerobic conditions during the synthetic procedure. Furthermore, the relatively low pH value of the reaction mixture renders thermodynamically unfavourable the reduction of Fe^{III} by the solvent (H_2O). Therefore the low values of the BVS (2.3–2.5) for the exolacunary Fe^{III} centre, shown in Table T2 (ESI†), can be explained by the fractional occupancy of the four crystallographic positions located at the "windows" of the cluster. This effect of the crystallographic disorder on the calculated BVS values of transition metals coordinated by oxo ligands has been previously reported.[15]

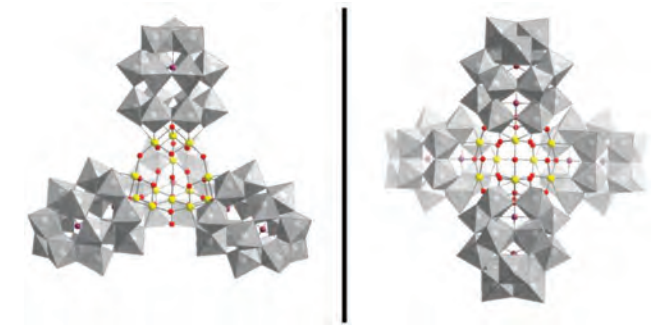

Fig. 2 Representations of the molecular structure of **1**. Left, representation viewed along one of the σ_v planes. Right, representation viewed along the same plane after performing a *ca.* 120° rotation around the axis perpendicular to that plane.

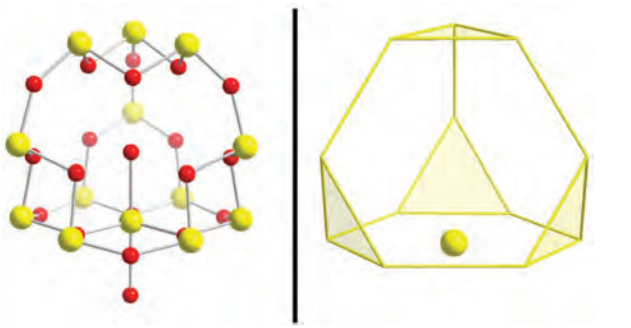

Fig. 3 Ball-and-stick (left) and polygonal (right) representations of the Fe-oxo core in **1**. The position of the exolacunary Fe^{III} centre is highlighted in the polygonal representation.

The coordination geometry of this exolacunary Fe^{III} centre is trigonal bipyramid as three bridging oxo ligands bind to the metal centre at equatorial positions while two aqua ligands occupy the axial positions. A small distortion of the bond distances is observed (0.3–0.5 Å) between the equatorial oxo ligands and the axial aqua ligands, a variation which have been ascribed to a difference in hapticity of the ligands in previously reported Fe-TMSPs.[16] The distances between the bridging hydroxo ligands and the Fe^{III} centres range from 1.87(1) Å to 1.98(1) Å while the corresponding Fe^{III}–O–Fe^{III} angles range from 141.8(6)° to 143.0(7)°. Moreover, the topology of the central cavity enclosed by the $\{Fe^{III}_{13}O_{20}\}$ core can be described as an Archimedean solid, *i.e.* a truncated tetrahedron.[17] This solid is thereby formed by removing the four vertices of the tetrahedron defined by the lines joining the four separate $\{\mu_4\text{-O}\}$ ligands connecting the Fe^{III} centres and one of the P^V centres in each of the $\{Fe^{III}_3P_2W_{15}\}$ units (Fig. 3). This idealised cavity is thus delimited by twelve short edges formed by the lines connecting neighbouring Fe^{III} centres in each $\{Fe^{III}_3P_2W_{15}\}$ unit and by six long edges formed by the lines connecting the Fe^{III} centres linked by bridging hydroxo ligands.

As discussed previously, an $\{Fe^{III}_{12}\}$ core is found in **3** which encloses a cavity of analogous topology as **1**'s, the main difference being the replacement of the exolacunary Fe^{III} centre by a central K^+ ion in **3**. Hence, the size of both cavities can be compared by measuring the distances between the triangular faces and their corresponding opposite hexagonal faces of the truncated tetrahedrons in both clusters. Accordingly, the average of these four distances in **1** is 5.65 Å while the same average in **3** has a similar value of 5.60 Å. The distances between the oxygen atom from the aqua ligand located at the centre of the cavity and the non-bridging hydroxo ligands in the $\{Fe^{III}_3P_2W_{15}\}$ units range from 3.02(1) Å to 3.06(2) Å while the analogous distances in **3**, *i.e.* the distances between the central K^+ and the equivalent hydroxo ligands, range from 3.03(1) Å to 3.08(1) Å.

In a similar fashion, the structure of **2** can also be described as an assembly of four $\{Fe^{III}_3P_2W_{15}\}$ units albeit connected by phosphato instead of hydroxo ligands. This change in bridging ligands, from $\{\mu_2\text{-OH}\}$ in **1** to $\{\mu_3\text{-}PO_4\}/\{\mu_4\text{-}PO_4\}$ in

2, does not affect the overall symmetry of the cluster which remains an idealised C_{3v}. Each of the phosphato ligands connects three $\{Fe^{III}{}_3P_2W_{15}\}$ units *via* three of their oxo centres, whereas in **1** the hydroxo bridges connect just two of those units. Four oxygen atoms, one from each of those phosphato ligands, are located in the interior of the central cavity, three of them binding to the exolacunary Fe^{III} centre. This Fe^{III} centre is statistically disordered over four different crystallographic positions which are in turn different to the positions occupied by the exolacunary centre in **1**. Two representations of the molecular structure of **2** are shown in Fig. 4. This polyanion can also be described as a discrete $\{Fe^{III}{}_{13}\}$ unit encapsulated by four trivacant $\{\alpha\text{-}P_2W_{15}\}$ units. Hence, the resulting $\{Fe^{III}{}_{13}O_{24}P_4\}$ core (Fig. 5) can be formulated as $[Fe^{III}\subset\{(PO_4)_4Fe^{III}{}_{12}O_3(OH)_9\}]^{12+}$ on the basis of BVS (see ESI†), electrochemical, microanalytical and analogous synthetic considerations to the ones discussed for the formation of **1**. This exolacunary Fe^{III} centre in **2** is octahedrally coordinated to three oxo ligands from one of the $\{Fe^{III}{}_3P_2W_{15}\}$ units and three of the "inner" oxo ligands belonging to separate phosphato ligands. A cubane motif, highlighted in Fig. 6, is formed by the exolacunary Fe^{III} centre the Fe^{III} centres from the nearest $\{Fe^{III}{}_3P_2W_{15}\}$ unit and the connecting oxo ligands. The three bond distances between the exolacunary Fe^{III} centre and the oxo ligands in the cubane range from 2.04(1) Å to 2.26(2) Å

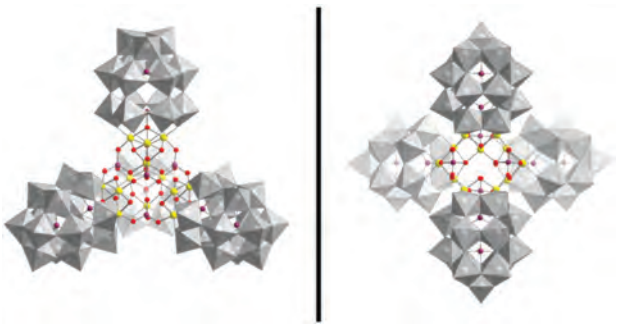

Fig. 4 Representations of the molecular structure of **2**. Left, representation viewed along one of the σ_v planes. Right, representation viewed along the same plane after performing a *ca.* 120° rotation around an axis perpendicular to that plane.

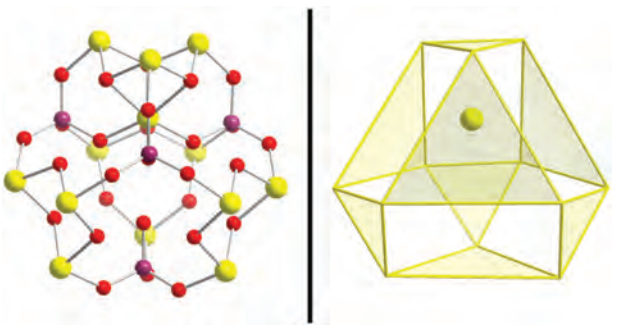

Fig. 5 Ball-and-stick (left) and polygonal (right) representations of the Fe–P-oxo core in **2**. The position of the exolacunary Fe^{III} centre is highlighted in the polygonal representation.

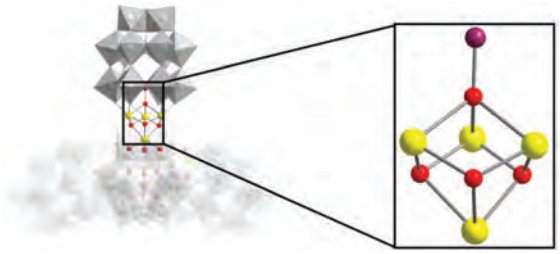

Fig. 6 Representation of the molecular structure of **2** highlighting the $\{Fe^{III}{}_3O_4\}$ cubane forming part of the central $\{Fe_{13}O_{24}P_4\}$ core.

while the corresponding Fe^{III}–O–Fe^{III} angles range from 90.2(7)° to 97.1(7)°. Furthermore, The Fe^{III}–O–Fe^{III} angles formed by the Fe^{III} centres in the $\{Fe^{III}{}_3P_2W_{15}\}$ and the oxo ligands connected solely to Fe^{III} centres unit range from 109.5(7)° to 110.2(6)° and from 92.3(6)° to 93.5(7)° for the angles including the oxo ligand which forms part of the templating $[PO_4]^{3-}$ anion. None of the oxygen atoms in the four bridging phosphato ligands is protonated, according to BVS calculations (ESI†), elemental analysis and charge balance considerations. Finally, the distances between the oxo centres in these bridging ligands and the Fe^{III} centres (excluding the exolacunary Fe^{III}) range from 1.91(1) Å to 1.94(1) Å while the corresponding P^V–O–Fe^{III} angles range from 130.1(8)° to 133.5(9)°.

The central cavity in the structure of **2** is delimited by the imaginary lines connecting the Fe^{III} centres in the $\{Fe^{III}{}_3P_2W_{15}\}$ units. The topology of this cavity, shown in Fig. 5, can be described as a semi-regular Archimedean solid, namely, an elongated cuboctahedron[17] formed by the twelve short edges that connect the Fe^{III} centres belonging to the same $\{\alpha\text{-}Fe^{III}{}_3P_2W_{15}\}$ units and the twelve longer edges that connect neighbouring Fe^{III} centres belonging to different $\{\alpha\text{-}Fe^{III}{}_3P_2W_{15}\}$ units. This geometrical description of the core in **2** allows us to compare the dimensions of the cavities in **1** and **2** by means of the distances between opposing faces of both solids.

Thus, the average of the distances between opposing triangular faces of the elongated cuboctahedron in **2** has a value, 7.10 Å, significantly greater than the equivalent average in **1**, 5.54 Å (Fig. 7). The exolacunary Fe^{III} centre occupies a different position within the core of the two clusters, *i.e.* inside the central cavity described by the elongated cuboctahedron in **2** but at the centre of one of the hexagonal faces forming the truncated tetrahedron in **1**. Finally, the two clusters also are

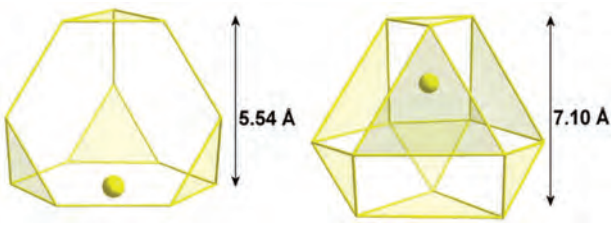

Fig. 7 Top, polygonal representations of the $\{Fe^{III}{}_{12}\}$ cores in **1** (left) and **2** (right) highlighting the distance between opposing polygonal faces.

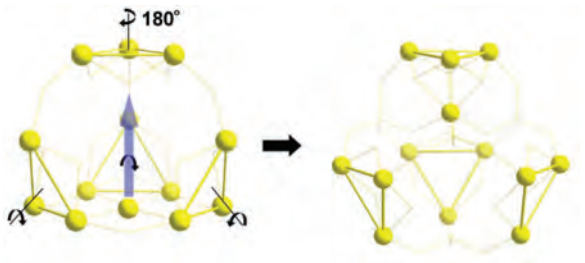

Scheme 2 Idealised symmetry and translational operations required to transform the core in **1** to the one in **2**. The ligand substitution step has been omitted for clarity.

structurally related in the sense that a three-step virtual manipulation of their molecular frameworks allows for their interconversion, as illustrated in Scheme 2. Hence, if the four $\{Fe^{III}{}_3P_2W_{15}\}$ units in **1** are rotated 180° around their respective C_3 axes, the exolacunary Fe^{III} centre is moved in a direction towards the opposite $\{Fe^{III}{}_3P_2W_{15}\}$ unit and all the hydroxo bridges are replaced by phosphato bridges, the structure of **2** is obtained. This conversion does not seem to correspond directly to an actual synthetic route as adding phosphate ions to aqueous solutions of **1** under a range of different synthetic conditions do not result in the crystallisation of **2**. Presumably, the robustness of the molecular framework of **1**, which seems to remain intact during the transformation of **1** into **3** in solution, explains the inability of the phosphato ligands to replace the hydroxo ligands under the explored synthetic conditions.

Electrochemistry

The electrochemical properties of **1** and **2** in aqueous solution were investigated by cyclic voltammetry (CV). Two voltammograms, obtained from aqueous solutions of the clusters at a pH value (4.4) close to the value at which the clusters form (5.0), are shown in Fig. 8. Starting from the anodic section of the voltammograms, the reduction of the Fe^{III} centres can be observed, in the case of **1**, as two ill-defined waves starting at

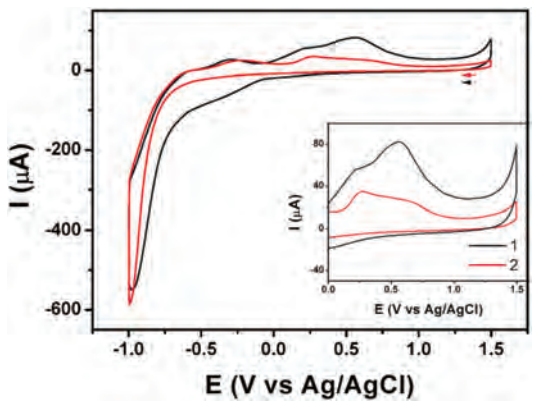

Fig. 8 Cyclic voltammograms (second cycle shown) of aqueous solutions of **1** (black line, [**1**] = 9 × 10^{-4} mol L^{-1}) and **2** (red line, [**2**] = 11 × 10^{-4} mol L^{-1}) at pH = 4.4 ($Na[CH_3COO]/H^+$, 0.1 M; Na_2SO_4, 0.2 M). The scan speed was 800 mV s^{-1} and the scan direction is indicated by the arrows.

−0.06 V. This stepwise reduction process has been previously observed in related Fe-POM clusters and explained on the basis of the electronic interaction between inequivalent Fe^{III} centres.[18] These are subsequently followed by a pronounced wave starting at −0.66 V which can be ascribed to the reduction of the W^{VI} centres. In the case of **2**, the redox waves associated to the reduction of the Fe^{III} centres are not detectable under the specific experimental conditions (pH) employed to record the voltammogram. The sharp wave originating at −0.71 V can be assigned to the reduction of the W^{VI} centres. Upon scan reversal, the reoxidation of these centres occurs at similar potentials for both clusters, a feature reflected on the waves peaking at −0.29 V and −0.22 V in **1**'s and **2**'s voltammograms respectively. Moving further towards the anodic potential region, a composite wave present in both voltammograms can be assigned to the reoxidation of the electrochemically generated Fe^{II} centres. These waves can be divided into two sections: a first peak at *ca.* +0.24 V and a second peak at +0.56 V, the latter being significantly more intense in **1**'s voltammogram. A demetalation process involving the Fe^{III} centres in related TMSPs has been proposed as the cause for these reoxidation waves.[19] Briefly, this process consists of the ejection of the electrochemically generated Fe^{II} centres from the cluster into the electrolyte solution by virtue of their increased lability with respect to the Fe^{III} centres. Upon reoxidation of these free Fe^{II} cations to Fe^{III} at the surface of the electrode, they return to the vacant positions in the cluster.

The number and position of both tungsten- and heterometal-centred redox waves observed in voltammetric measurements can vary considerably as a function of the pH.[20] Hence, we decided to investigate the electrochemical behaviour of both clusters in aqueous solution at a lower pH value (2.2). In order to ensure that the polyanions were stable in the acidified electrolyte a series of UV-Vis spectra were obtained from the corresponding solutions at increasing time intervals after preparation. These spectra, shown in Fig. S6 (ESI†), confirm that both clusters are stable at pH 2.2 for the duration of a typical CV experiment.

The voltammograms of **1** and **2** obtained at pH 2.2 are shown in Fig. 9. An inspection of these plots, starting from the highest anodic potential (+1.5 V) and moving towards the cathodic end of the voltammogram (−1.0 V), reveals the presence of two consecutive waves, peaking at potential values of *ca.* +0.17 V and *ca.* −0.11 V respectively for both clusters. These waves, which are considerably more intense in **1**'s voltammogram, can be assigned to the stepwise reduction of the Fe^{III} centres while their corresponding reoxidation waves can be observed on the anodic section of the voltammogram upon scan reversal. However, this reoxidation process occurs sequentially in the case of **1**, as reflected on the two ill-defined waves observed at +0.23 V and +0.70 V, while the oxidation of the electrochemically generated Fe^{II} centres from **2** seems to occur in one single step, causing the sharp wave which peaks at +0.87 V. A comparison of the voltammograms of **1** shown in Fig. 8 and 9 suggests that the redox processes associated to the Fe^{III} centres are strongly dependent on the value of pH. The

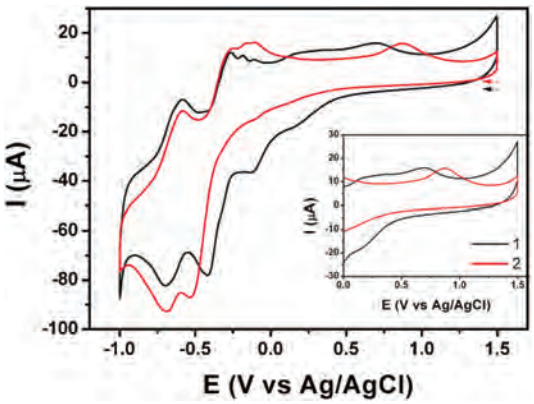

Fig. 9 Cyclic voltammograms (second cycle shown) of aqueous solutions of **1** (black line, [**1**] = 1 × 10^{-4} mol L^{-1}) and **2** (red line, [**2**] = 2 × 10^{-4} mol L^{-1}) at pH = 2.2 ($Na[CH_3COO]/H^+$, 0.1 M; Na_2SO_4, 0.2 M). The scan speed was 800 mV s^{-1} and the scan direction is indicated by the arrows.

change of the pH value from 4.4 to 2.2 results in a 220 mV cathodic shift of the onset of the Fe^{III} reduction and in a 140 mV anodic shift of the current peak assigned to the corresponding reoxidation. These variations are consistent with reports describing the effect of solution pH on the electrochemistry of related Fe-POM clusters.[21]

The wave couples assigned to the W-centred redox processes are better defined in the plots shown in Fig. 9 (pH 2.2) than in the ones shown in Fig. 8 (pH 4.4). This effect is caused by the dependence of the position and intensity of these waves on the protonation of the cluster, a process coupled to these electron transfers. Hence, two consecutive waves caused by the reduction of the W^{VI} centres can be observed in the cathodic regions of both voltammograms. Their potential values differ slightly between the two clusters: the first wave peaks at −0.42 V in **1** and −0.53 V in **2** while the second wave peaks at *ca.* −0.70 V for both clusters. Furthermore, the reoxidation wave associated to the latter process peaks at *ca.* −0.58 V in both clusters upon scan reversal, therefore completing a wave couple ascribed to a well defined, quasi-reversible, process. However, the reoxidation wave associated to the first reduction of W^{VI} centres in both clusters is actually a composite wave, comprised of three poorly defined redox couples contained in a potential region located between −0.29 V and −0.06 V.

A comparison of **1**'s and **2**'s voltammograms obtained after one or two potential scans (Fig. S2†) show no significant differences in the position nor the intensity of the redox waves, save for an slight increase in the current intensity detected in the reoxidation of the Fe^{III} centres in **2**. This similarity of the voltammograms is a further reflection of the stability of the clusters in aqueous solution under this particular range of experimental conditions.

ESI-MS analysis

During the past decade, ESI-MS has proved to be a valuable tool in our efforts to determine unambiguously the integrity of a variety of TMSPs and the composition of their metallic cores.[22]

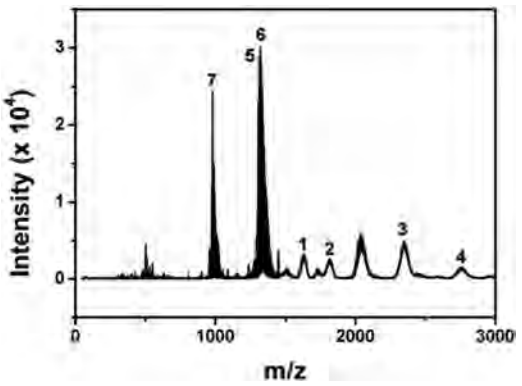

Fig. 10 Mass spectrum of a H_2O–CH_3CN solution of **1**. A number of relevant envelopes are labelled while their corresponding *m*/*z* values and assignments are listed in Table 3.

Table 3 Assignments and *m*/*z* values for the highlighted envelopes in Fig. 10. Simulated isotopic patterns and sections of the spectrum showing these envelopes are given in Fig. S7–S13 (ESI)

Env.	Formula	Sim. (*m*/*z*)	Obs. (*m*/*z*)
1	$\{Na_{16}H_4[\mathbf{1}]\}^{10-}$	1629.98	1629.88
2	$\{Na_{18}H_3[\mathbf{1}]\}^{9-}$	1816.08	1815.95
3	$\{Na_{20}H_3(H_2O)_2[\mathbf{1}]\}^{7-}$	2346.54	2347.36
4	$\{Na_{22}H_2(H_2O)_5[\mathbf{1}]\}^{6-}$	2754.13	2754.09
5	$\{Na_9H_2(H_2O)[(P_2W^{V}{}_2W^{VI}{}_{13}O_{56})]\}^{3-}$	1313.95	1313.90
6	$\{Na_9H_5(H_2O)_2[(P_2W^{V}{}_5W^{VI}{}_{10}O_{56})]\}^{3-}$	1320.97	1320.90
7	$\{Na_8H_4(H_2O)[(P_2W^{V}{}_4W^{VI}{}_{11}O_{56})]\}^{4-}$	980.22	980.17

Therefore, this analytical technique was employed to assess further the composition of **1**'s and **2**'s molecular frameworks.

Crystals of Na_{30}-**1** were dissolved in a CH_3CN–H_2O mixture (95 : 5) and introduced in the spectrometer *via* electrospray injection to obtain negative ion mass spectra. The spectrum in Fig. 10 shows a number of envelopes which can be assigned to ionic species derived from **1**. These assignments are summarised in Table 3. Four of them (1–4) are ascribed to adducts formed by **1** and Na^+ cations in different protonation states. The charge of these adducts range from 6- to 10- and their formulae are abbreviated as follows: $\{Na_{16}H_4\text{-}\mathbf{1}\}^{10-}$, $\{Na_{18}H_3\text{-}\mathbf{1}\}^{9-}$, $\{Na_{20}H_3(H_2O)_2\text{-}\mathbf{1}\}^{7-}$ and $\{Na_{22}H_2(H_2O)_5\text{-}\mathbf{1}\}^{6-}$. Hence, these envelopes provide additional support for the proposed formulation of **1** based on crystallographic and elemental analyses. Furthermore, they provide evidence for the stability of the cluster in the gas phase even though the high ionization temperature (180 °C) caused partial fragmentation of the species. Envelopes 5 to 7 are assigned to fragments containing the lacunary precursor $\{P_2W_{15}\}$ reduced and protonated to different extents.

In the case of **2**, mass spectra were recorded from solutions of crystals of Na_{33}-**2** in CH_3CN–H_2O (95 : 5) mixtures under similar experimental conditions to those used to obtain **1**'s spectrum. The resulting spectrum (Fig. 11) shows a series of distribution envelopes which can be assigned to a number of charged species derived from **2** while Table 4 summarises those assignments. Four of those envelopes, located at the high

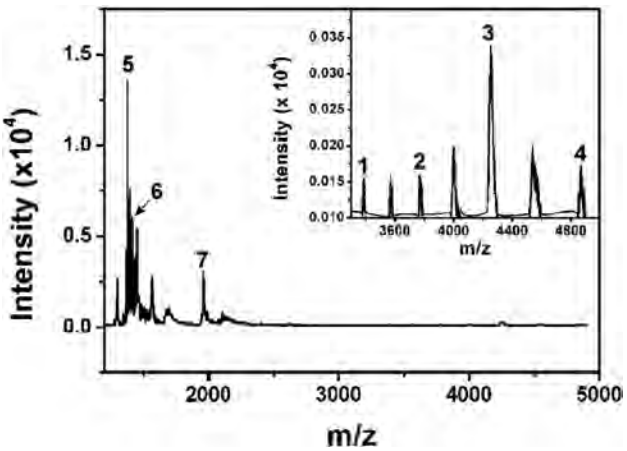

Fig. 11 Mass spectrum of a H_2O–CH_3CN solution of **2**. A number of relevant envelopes are labelled while their corresponding *m*/*z* values and assignments are listed in Table 4.

Table 4 Assignments and *m*/*z* values for the highlighted envelopes in Fig. 11. Simulated isotopic patterns and sections of the spectrum showing a selection of these envelopes are given in Fig. S14–S16 (ESI)

Env.	Formula	Sim. (*m*/*z*)	Obs. (*m*/*z*)
1	$\{Na_{54}H_2(H_2O)_{21}[\mathbf{2}]_2\}^{10-}$	3391.2	3391.42
2	$\{Na_{55}H_2(H_2O)_{20}[\mathbf{2}]_2\}^{9-}$	3774.5	3774.61
3	$\{Na_{55}H_3(H_2O)_{24}[\mathbf{2}]_2\}^{8-}$	4255.5	4255.31
4	$\{Na_{55}H_4(H_2O)_{25}[\mathbf{2}]_2\}^{7-}$	4866.1	4866.32
5	$\{Na_6H_5(Fe^{II}{}_3P_2W^{V}{}_2W^{VI}{}_{13}O_{56}(OH)_6)]\}^{3-}$	1375.91	1375.89
6	$\{Na_7H_3(H_2O)(Fe^{II}{}_2Fe^{III}P_2W^{VI}{}_{15}O_{56}(OH)_5(PO_4)]^{3-}$	1414.89	1414.88
7	$\{Na_8H_3(H_2O)(P_2W^{V}W^{VI}{}_{14}O_{56})\}^{2-}$	1959.94	1959.88

m/*z* range of the spectrum, can be ascribed to dimeric assemblies of **2**. The condensed formulae of these adducts are $\{Na_{54}H_2(H_2O)_{21}[\mathbf{2}]_2\}^{10-}$ (1), $\{Na_{55}H_2(H_2O)_{20}[\mathbf{2}]_2\}^{9-}$ (2), $\{Na_{55}H_3(H_2O)_{24}[\mathbf{2}]_2\}^{8-}$ (3) and $\{Na_{55}H_4(H_2O)_{25}[\mathbf{2}]_2\}^{7-}$ (4). The presence of these dimers in the spectrum supports the proposed formulation of **2** and provides an insight into the stability of the cluster in the gas phase.

In addition, a monomeric fragment in which one of the terminal oxo ligands bound to a Fe centre is replaced by a phosphato ligand, can be assigned to the envelop observed at *m*/*z* 1414.88 (6). The $\{Fe_3P_2W_{15}\}$ unit is also detected from the envelope observed at *m*/*z* 1375.89 (5). Similar to the case of **1**'s spectrum, an envelope at *m*/*z* 1959.88 (7) can be ascribed to the lacunary precursor $\{P_2W_{15}\}$.

Conclusions

In conclusion, we have reported the syntheses, structural and solution investigation of two novel nano-sized clusters $[Fe^{III}{}_{13}P_8W_{60}O_{227}(OH)_{15}(H_2O)_2]^{30-}$ (**1**) and $[Fe^{III}{}_{13}P_8W_{60}O_{224}(OH)_{12}(PO_4)_4]^{33-}$ (**2**) which belong to the TMSP family. Careful investigation of the experimental variables led to the formation of the two nano-tetrahedral species which had previously evaded detection and adopt metallic cores of different size and interesting topology. The Fe core in **1** exhibits a truncated tetrahedron (0.56 nm) while in **2** forms an elongated cuboctahedron (0.76 nm) with the thirteenth iron centre located in different positions within the cores. Furthermore, we demonstrated the selective K^+ entrapment which triggers the expulsion of the exolacunary Fe^{III} centre from the core of compound **1**. The potassium cations have proved to fulfill the appropriate requirements in terms of size and coordination ability for the process to take place. The preparation of such clusters improves our understanding of the relationship between the topology and composition of these oxometallic cores and their ability to undergo framework transformations under marginal structural rearrangement. Electrochemical and ESI-MS studies have proved to be extremely useful for the unambiguous identification and characterization of their complex architecture. In the future, we will attempt to extend our studies in the discovery of nanosized molecular systems, exhibiting controlled functionality triggered by external and/or internal stimuli, to other combinations of first-row transition metals and polyoxometalate lacunary ligands.

Experimental

Materials

All reagents were used as purchased without further purification while $Na_{12}[\alpha\text{-}P_2W_{15}O_{56}]\cdot 18H_2O$ was synthesized according to the published procedure.[23] For details regarding all instrumentation used, see the ESI.†

Synthesis

Synthesis of $Na_{30}[Fe^{III}{}_{13}P_8W_{60}O_{227}(OH)_{15}(H_2O)_2]\cdot 56H_2O$ (Na_{30}-1). $FeCl_3\cdot 6H_2O$ (1.0 g, 3.7 mmol) was dissolved in 30 mL of 2 M aqueous NaCl. $Na_{12}[\alpha\text{-}P_2W_{15}O_{56}]\cdot 18H_2O$ (6.0 g, 1.4 mmol) was added to the turbid dark yellow solution in small portions under vigorous stirring over a period of 15 min. This reaction mixture was allowed to stir for a further 5 min before adjusting the pH to 5.00 by dropwise addition of 5 M aqueous NaOH. The dark red limpid solution was then heated at 85 °C for 5 min, filtered hot into a wide-neck 100 mL conical flask and finally placed in a temperature-controlled crystallisation room (18 ± 1 °C). Hexagonal dark red plates formed overnight and were isolated from the mother liquor after 3 d. Yield: 1.771 g, 0.100 mmol, 30% based on W. $Na_{30}[Fe^{III}{}_{13}P_8W_{60}O_{227}(OH)_{15}(H_2O)_2]\cdot 56H_2O$, $Fe_{13}H_{131}Na_{30}O_{300}P_8W_{60}$, MW = 17 625.55 g mol^{-1}. Characteristic IR bands (cm^{-1}): 694 (vs), 795(s), 871 (vs), 900 (s), 938 (sh); 1080 (vs). ^{31}P-NMR (D_2O), δ = −15.5 ppm (85% H_3PO_4, 0.00 ppm). UV absorption: $\lambda(O \rightarrow W)$ = 278 nm, $\varepsilon = 22.14 \times 10^4$ mol^{-1} L cm^{-1}. Elemental analysis (%) for the dehydrated material $Fe_{13}H_{19}Na_{30}O_{244}P_8W_{60}$, calculated (found): Na, 4.15 (4.22); Fe, 4.37 (4.44); W, 66.38 (66.81). Water content (%), crystallographic (TGA, 25–200 °C, N_2 atmosphere): 5.74 (5.73).

Synthesis of $Na_{33}[Fe^{III}{}_{13}P_8W_{60}O_{224}(OH)_{12}(PO_4)_4]\cdot 67H_2O$ (Na_{33}-2). H_3PO_4 (50 μL, 0.73 mmol, 85% wt. in H_2O) was

added to 15 mL of 2 M aqueous NaCl followed by $FeCl_3{\cdot}6H_2O$ (0.50 g, 1.9 mmol). $Na_{12}[P_2W_{15}O_{56}]{\cdot}18H_2O$ (3.0 g, 0.7 mmol) was slowly added over 10 min to the cloudy dark yellow solution under vigorous stirring. The resultant light brown turbid solution was allowed to stir for a further 5 min before carefully adjusting the pH to 5.00 by adding small volumes of first 5 M and then 2.5 M aqueous NaOH. The pH of the brown suspension was maintained between 4.95 and 5.05 for 10 min through dropwise addition of 1 M aqueous NaOH. Thereafter, the reaction mixture was heated at 85 °C for 5 min and the resulting clear dark brown solution was filtered hot and finally placed in a temperature-controlled crystallisation room (18 ± 1 °C). Brown block crystals were isolated from the light brown mother liquor on the following day. Yield: 0.851 g, 0.047 mmol, 28% based on W. $Na_{33}[Fe^{III}{}_{13}P_8W_{60}O_{224}(OH)_{12}(PO_4)_4]{\cdot}67H_2O$, $Fe_{13}H_{146}Na_{33}O_{319}P_{12}W_{60}$, MW = 18 138.53 g mol^{-1}. Characteristic IR bands (cm^{-1}): 696 (vs); 777 (vs), 870 (m), 905 (s), 943 (sh); 956 (s); 1082 (s). ^{31}P-NMR (D_2O), δ = −16.6 ppm (85% H_3PO_4, 0.0 ppm). UV absorption: $\lambda(O \rightarrow W)$ = 280 nm, $\varepsilon = 21.8 \times 10^4$ mol^{-1} L cm^{-1}. Elemental analysis (%) for the dehydrated material $Fe_{13}H_{12}Na_{33}O_{252}P_{12}W_{60}$, calculated (found): Na, 4.43 (4.48); Fe, 4.28 (4.25); W, 65.15 (65.24). Water content (%), crystallographic (TGA, 25–200 °C, N_2 atmosphere): 6.64 (5.84).

Synthesis of $K_{21}Na_8[KFe_{12}(OH)_{18}(\alpha\text{-}1,2,3\text{-}P_2W_{15}O_{56})_4]$. The pH value of 10 mL 0.1 M aqueous KCl was adjusted to 3.0 *via* the addition of a small volume of 0.1 M aqueous HCl. Crystals of Na_{30}-**1** (0.2 g, 0.011 mmol) were added to the stirring solution and the resulting suspension was quickly heated until complete dissolution. The hot yellow solution was filtered at once into a narrow-neck 25 mL conical flask and placed in a temperature-controlled crystallisation room (18 ± 1 °C). Yellow block crystals formed overnight and their identity was confirmed as $K_{21}Na_8$-**3** by several unit cell checks. Yield: 0.035 g, 1.9 μmol, 18% based on W.

Acknowledgements

L.C. thanks the EPSRC for funding (grants EP/H024107/1; EP/I033459/1; EP/J015156/1) and the EU FP7 Micreagents (318671) and the Royal-Society Wolfson Foundation for a Merit Award, and the University of Glasgow.

Notes and references

1 D.-L. Long, R. Tsunashima and L. Cronin, *Angew. Chem., Int. Ed.*, 2010, **49**, 1736–1758.
2 H. N. Miras, J. Yan, D.-L. Long and L. Cronin, *Chem. Soc. Rev.*, 2012, **41**, 7403–7430.
3 O. Oms, A. Dolbecq and P. Mialane, *Chem. Soc. Rev.*, 2012, **41**, 7497–7536.
4 C. Lydon, M. M. Sabí, M. D. Symes, D.-L. Long, M. Murrie, S. Yoshii, H. Nojiri and L. Cronin, *Chem. Commun.*, 2012, **48**, 9819–9821.
5 Y. Sakai, K. Yoza, C. N. Kato and K. Nomiya, *Dalton Trans.*, 2003, 3581–3586.
6 Y. Sakai, K. Yoza, C. N. Kato and K. Nomiya, *Chem.–Eur. J.*, 2003, **9**, 4077–4083.
7 U. Kortz, S. S. Hamzeh and N. A. Nasser, *Chem.–Eur. J.*, 2003, **9**, 2945–2952.
8 C. P. Pradeep, D.-L. Long, P. Kögerler and L. Cronin, *Chem. Commun.*, 2007, 4254–4256.
9 (*a*) L. H. Bi, U. Kortz, S. Nellutla, A. C. Stowe, J. van Tol, N. S. Dalal, B. Keita and L. Nadjo, *Inorg. Chem.*, 2005, **44**, 896–903; (*b*) B. Botar, Y. V. Geletii, P. Kögerler, D. G. Musaev, K. Morokuma, I. A. Weinstock and C. L. Hill, *J. Am. Chem. Soc.*, 2006, **128**, 11268–11277; (*c*) B. Botar, P. Kögerler and C. L. Hill, *Inorg. Chem.*, 2007, **46**, 5398–5403; (*d*) X. Zhao, Y.-G. Li, Y.-H. Wang and E.-B. Wang, *Transition Met. Chem.*, 2008, **33**, 323–330; (*e*) Y. Liu, J. Shang, G. Xue, H. Hu, F. Fu and J. Wang, *J. Cluster Sci.*, 2007, **18**, 205–216; (*f*) N. H. Nsouli, S. S. Mal, M. H. Dickman, U. Kortz, B. Keita, L. Nadjo and J. M. Clemente-Juan, *Inorg. Chem.*, 2007, **46**, 8763–8770; (*g*) T. M. Anderson, W. A. Neiwert, K. I. Hardcastle and C. L. Hill, *Inorg. Chem.*, 2004, **43**, 7353–7358.
10 (*a*) C. Pichon, A. Dolbecq, P. Mialane, J. Marrot, E. Rivière and F. Sécheresse, *Dalton Trans.*, 2008, 71–76; (*b*) J.-W. Zhao, H.-P. Jia, J. Zhang, S.-T. Zheng and G.-Y. Yang, *Chem.–Eur. J*, 2007, **13**, 10030–10045.
11 W. Chen, Y. Li, Y. Wang, E. Wang and Z. Zhang, *Z. Anorg. Allg. Chem.*, 2009, **635**, 1678–1687.
12 M. Ibrahim, Y. H. Lan, B. S. Bassil, Y. X. Xiang, A. Suchopar, A. K. Powell and U. Kortz, *Angew. Chem., Int. Ed.*, 2011, **50**, 4708–4711.
13 Q. Wu, Y.-G. Li, Y.-H. Wang, E.-B. Wang, Z.-M. Zhang and R. Clérac, *Inorg. Chem.*, 2009, **48**, 1606–1612.
14 P. Mialane, A. Dolbecq, J. Marrot, E. Rivière and F. Sécheresse, *Angew. Chem., Int. Ed.*, 2003, **42**, 3523–3526.
15 R. M. Wood and G. J. Palenik, *Inorg. Chem.*, 1998, **37**, 4149–4151.
16 X. Zhang, Q. Chen, D. C. Duncan, R. J. Lachicotte and C. L. Hill, *Inorg. Chem.*, 1997, **36**, 4381–4386.
17 S. M. Rajtmajer, A. Miličevic, N. Trinajstić, M. Randić and D. Vukičević, *J. Math. Chem.*, 2006, **39**, 119–132.
18 I. M. Mbomekalle, B. Keita, L. Nadjo, P. Berthet, K. I. Hardcastle, C. L. Hill and T. M. Anderson, *Inorg. Chem.*, 2003, **42**, 1163–1169.
19 B. Keita, I. M. Mbomekalle, L. Nadjo, T. M. Anderson and C. L. Hill, *Inorg. Chem.*, 2004, **43**, 3257–3263.
20 (*a*) B. Keita, Y.-W. Lu, L. Nadjo and R. Contant, *Electrochem. Commun.*, 2000, **2**, 720–726; (*b*) B. S. Bassil, S. Nellutla, U. Kortz, A. C. Stowe, J. van Tol, N. S. Dalal, B. Keita and L. Nadjo, *Inorg. Chem.*, 2005, **44**, 2659–2665; (*c*) L. Lisnard, P. Mialane, A. Dolbecq, J. Marrot, J. M. Clemente-Juan, E. Coronado, B. Keita, P. de Oliveira, L. Nadjo and F. Sécheresse, *Chem.–Eur. J.*, 2007, **13**, 3525–3536.
21 (*a*) B. Botar, Y. V. Geletii, P. Kögerler, D. G. Musaev, K. Morokuma, I. A. Weinstock and C. L. Hill, *Dalton Trans.*, 2005, 2017–2021; (*b*) I. M. Mbomekalle, R. Cao,

K. I. Hardcastle, C. L. Hill, M. Ammam, B. Keita, L. Nadjo and T. M. Anderson, *C. R. Chim.*, 2005, **8**, 1077–1086; (*c*) U. Kortz, M. G. Savelieff, B. S. Bassil, B. Keita and L. Nadjo, *Inorg. Chem.*, 2002, **41**, 783–789; (*d*) R. Contant, M. Abbessi, J. Canny, A. Belhouari, B. Keita and L. Nadjo, *Inorg. Chem.*, 1997, **36**, 4961–4967.

22 (*a*) H. N. Miras, E. F. Wilson and L. Cronin, *Chem. Commun.*, 2009, 1297–1311; (*b*) H. N. Miras, D.-L. Long, P. Kögerler and L. Cronin, *Dalton Trans.*, 2008, 214–221; (*c*) M. N. Corella-Ochoa, H. N. Miras, D.-L. Long and L. Cronin, *Chem.–Eur. J.*, 2012, **18**, 13743–13754; (*d*) H. N. Miras, H. Y. Zang, D.-L. Long and L. Cronin, *Eur. J. Inorg. Chem.*, 2011, 5105–5111.

23 R. Contant, W. G. Klemperer and O. Yaghi, in *Inorganic Syntheses*, John Wiley & Sons, Inc., 2007, pp. 104–111.

24 R. C. Clark and J. S. Reid, *Acta Crystallogr., Sect. A: Found. Crystallogr.*, 1995, **51**, 887–897.

25 R. H. Blessing, *Acta Crystallogr., Sect. A: Found. Crystallogr.*, 1995, **51**, 33–38.

26 G. Sheldrick, *Acta Crystallogr., Sect. A: Found. Crystallogr.*, 2008, **64**, 112–122.

27 L. Farrugia, *J. Appl. Crystallogr.*, 1999, **32**, 837–838.